Cancer Cell
Article

Cooperativity within and among Pten, p53, and Rb Pathways Induces High-Grade Astrocytoma in Adult Brain

Lionel M.L. Chow,[1,5] Raelene Endersby,[1] Xiaoyan Zhu,[1] Sherri Rankin,[1] Chunxu Qu,[2] Junyuan Zhang,[1] Alberto Broniscer,[3] David W. Ellison,[4] and Suzanne J. Baker[1,*]
[1]Department of Developmental Neurobiology
[2]Hartwell Center for Bioinformatics and Biotechnology
[3]Department of Oncology
[4]Department of Pathology
St. Jude Children's Research Hospital, Memphis, TN 38105, USA
[5]Department of Hematology/Oncology, Cincinnati Children's Hospital Medical Center, Cincinnati, OH 45229, USA
*Correspondence: suzanne.baker@stjude.org
DOI 10.1016/j.ccr.2011.01.039

SUMMARY

Mutations in the *PTEN*, *TP53*, and *RB1* pathways are obligate events in the pathogenesis of human glioblastomas. We induced various combinations of deletions in these tumor suppressors in astrocytes and neural precursors in mature mice, resulting in astrocytomas ranging from grade III to grade IV (glioblastoma). There was selection for mutation of multiple genes within a pathway, shown by somatic amplifications of genes in the PI3K or Rb pathway in tumors in which *Pten* or *Rb* deletion was an initiating event. Despite multiple mutations within PI3K and Rb pathways, elevated Mapk activation was not consistent. Gene expression profiling revealed striking similarities to subclasses of human diffuse astrocytoma. Astrocytomas were found within and outside of proliferative niches in the adult brain.

INTRODUCTION

High-grade gliomas (HGGs), which are WHO grade III and IV tumors, have a uniformly poor outcome with the most aggressive form, glioblastoma, a grade IV diffuse astrocytic tumor, bearing a long-term survival of less than 10% (Louis et al., 2007). Animal models that more accurately reflect HGG biology are needed to advance our understanding of this disease as well as to allow for more accurate preclinical testing of new treatment options.

The molecular pathogenesis of glioblastoma has been studied in detail, including high-resolution microarray analyses to identify copy number (CN) imbalances and gene expression signatures as well as in-depth sequence analyses to identify recurrent targets of mutation. These studies concluded that glioblastoma formation requires dysregulation in three core pathways: the receptor tyrosine kinase (RTK)/phosphatidylinositol 3′-kinase (PI3K)/AKT axis, p53 signaling, and RB-mediated control of cell cycle progression (Cancer Genome Atlas Research Network, 2008; Parsons et al., 2008). Genetic aberrations affecting intermediates of all three pathways are identified in virtually all glioblastomas. For the RTK/PI3K pathway, biallelic inactivation of *PTEN* through mutation coupled with LOH of chromosome (Chr) 10q is a common mechanism in glioblastoma to abrogate the major negative regulator restraining PI3K activation. The most common RTK target of mutation is amplification of *EGFR*, often coupled with intragenic deletion resulting in a constitutively activated form. p53 signaling is dysregulated frequently by biallelic inactivation of *TP53*, or in some cases by *HDM2* amplification. Homozygous deletions of *CDKN2A* simultaneously remove p14ARF, a negative regulator of p53 signaling, as well as INK4A,

Significance

Induced gene deletion in astrocytes and progenitors in mature brain, the developmental setting in which high-grade astrocytomas (HGAs) most commonly arise, showed selective cooperativity among tumor suppressors. *Tp53* deletion was required for HGA formation induced by deletion of *Pten*, *Rb1*, or combined *Pten*; *Rb1* deletion. Tumor latency and secondary mutations varied depending on the specific genes deleted. HGAs contained a spectrum of focal and large-scale somatic mutations relevant to human disease, and recapitulated all three gene expression subgroups previously identified in human gliomas by association with prognosis. Induction of Cre activity was widespread in astrocytes and restricted to limited populations of neural progenitors in adult brain, suggesting that astrocytomas can develop outside of proliferative niches, but with lower efficiency.

a key regulator of the RB-mediated G_1 checkpoint, thus impacting both p53 and RB pathways. Mutations in *RB1* are also found in glioblastoma (Cancer Genome Atlas Research Network, 2008; Parsons et al., 2008).

The effects of *Pten*, *Rb1*, or *Tp53* deletion in the mouse brain have been described through the use of mouse lines expressing *Cre* specifically in the brain. For the most part the phenotype obtained is cell-type and developmental-stage specific. For example, deletion of *Pten* in neural stem and progenitor cells resulted in expansion of the stem cell niche, a proliferative advantage in the progenitor cell population as well as migration defects causing a disruption in the laminar structure of the cortex (Gregorian et al., 2009; Groszer et al., 2001). In contrast, ablation of *Pten* in postmitotic cerebellar neurons resulted in cellular hypertrophy (Backman et al., 2001; Kwon et al., 2001; Marino et al., 2002). Pten null astrocytes showed evidence of hypertrophy and proliferation (Fraser et al., 2004; Wei et al., 2006) and abnormal migration (Yue et al., 2005). In the case of *Rb1*, conditional ablation at E9 in the telencephalon or the whole brain resulted in cell cycle defects characterized primarily by increased proliferation (Ferguson et al., 2002; MacPherson et al., 2003). Conditional deletion of *Tp53* combined with haploinsufficiency of *Nf1* and *Pten*, or deletion of *Nf1*, generated high-grade astrocytomas (HGAs) (Alcantara Llaguno et al., 2009; Kwon et al., 2008; Zheng et al., 2008). In contrast an intragenic deletion of *Tp53* encoding a mutant protein, induced in embryonic brain, was sufficient to cause malignant astrocytomas in mid-adulthood (Wang et al., 2009).

Although the exact histogenesis of gliomas is still a matter of some controversy, there is agreement that neural progenitor cells or mature astrocytes are likely candidates (Louis et al., 2007). We recently reported the characterization of *GFAP-CreER* mice with inducible targeting of approximately 50% of mature astrocytes, and less than 1% of neural precursor cells located in the subventricular zone (SVZ) and subgranular zone (SGZ) of the dentate gyrus (Chow et al., 2008). Here, we used this *GFAP-CreER* mouse line to study the tumor suppressor function of *Pten*, *Tp53*, and *Rb1* in the development of HGAs in mature brain because this is the context in which the majority of glioblastomas arise.

RESULTS

Minimal Effects of *Pten* Deletion in Mature Astrocytes

We generated *GFAP-CreER*^{TM}A (hereafter referred to as *CreER*); *Pten*$^{loxP/loxP}$ mice to investigate the effect of *Pten* loss in mature astrocytes. Cre activity was transiently induced in developmentally mature mice by tamoxifen administration after postnatal day (P) 21 (range P20–P45). Recombination and inactivation of *Pten* were confirmed by real-time PCR (see Figure S1A available online). Conditional deletion of *Pten* in mature brain did not reduce survival (Figure S1B) or disrupt brain architecture (Figures 1A–1C). There was a modest increase in Gfap expression in the brains of *Pten* conditional knockout (cKO) mice (Figures 1A–1F; Figure S1C, lanes 7–9), a feature also observed in primary cultures of Pten null astrocytes (data not shown). However, we did not detect astrocyte hypertrophy or hyperproliferation (data not shown).

Pten is the central negative regulator of the PI3K/Akt pathway (Chow and Baker, 2006). In rare Pten null granule neurons of the dentate gyrus that were targeted by this *CreER* strain, we detected the expected increase in phosphorylation of Akt (pAkt) at S473 or phosphorylation of S6 (pS6) at S235 and S236, indicating hyperactivity of the PI3K/Akt pathway (Figures S1D–S1I, arrows). However, western blot analyses of cortical lysates and immunohistochemistry (IHC) did not detect any perturbations in pathway signaling induced by *Pten* deletion in astrocytes (Figures 1G–1I; Figure S1C). Therefore, inactivation of *Pten* in adult astrocytes did not induce detectable activation of PI3K signaling and, accordingly, did not lead to an overt phenotype or tumor predisposition.

Combined Inactivation of *Pten* and *Tp53* Induced HGA

Highly penetrant HGAs were induced in *CreER*; *Pten*$^{loxP/loxP}$; *Tp53*$^{loxP/loxP}$ compound mice, hereafter termed *Pten*; *p53* cKO mice. Cre activity was induced in adult mice as described above. *Pten*; *p53* cKO mice had a significantly reduced survival compared to *Pten* cKO mice, or to *Pten*$^{loxP/+}$; *p53* cKO mice (Figure 2A). Fifty-five of 63 (87%) *Pten*; *p53* cKO brains harbored tumors within the spectrum of HGA, showing a range of histopathological features. Approximately 25% of tumors were classified as glioblastomas, on the basis that they featured scattered cells with an astrocytic phenotype, mitotic activity, cytological pleomorphism, including in some cases a substantial number of multinucleated giant cells (Figure 2B), necrosis (Figure 2C), and/or microvascular proliferation (Figure 2D). Approximately 25% of tumors were anaplastic astrocytomas with myxoid degeneration, a feature more commonly observed in pediatric gliomas than adult (Figure 2E). Half of the tumors were diffuse anaplastic astrocytomas, demonstrating infiltrating tumor cells (Figure 2F) and a focal astrocytic phenotype. In some cases there was extensive parenchymal infiltration combined focally with the architectural and cytological features of gliomatosis (Figure 2G). PCR analysis confirmed inactivation of the *Tp53* locus (Figure S2), and Pten IHC showed that tumor cells were Pten null (Figures 2H–2J), highlighting invasion by tumor cells of perivascular spaces (Figure 2I), leptomeninges (Figure 2J), and parenchyma.

Tumors consistently showed elevated pAkt (Figure 3A), and were highly proliferative, as shown by Ki67 IHC (Figure 3B). Active Caspase-3, a marker of apoptosis, was also detectable in most tumors (Figure 3C). Immunophenotyping of the tumors revealed Gfap and S100β immunoreactive tumor cells in varying proportions (Figures 3D; data not shown). Neurofilament (light-chain) IHC was negative in tumor cells (Figure 3E). Nestin, a marker of neural progenitor cells (Brustle and McKay, 1995), was also expressed in tumors (Figure 3F).

Tumors Developed within and outside of Proliferative Niches

The location of tumors within the CNS included all regions of the forebrain, midbrain, hindbrain, and spinal cord, and did not correlate to different histopathological features. Many tumors were contiguous with regions rich in neural progenitor cells, such as the SVZ, the rostral migratory stream (RMS), and SGZ of the dentate gyrus (Figures S3A and S3B). When tumors were not macroscopically evident, serial sectioning and H&E frequently revealed small groups of tumor cells invading through white matter tracts adjacent to zones rich in neural progenitors,

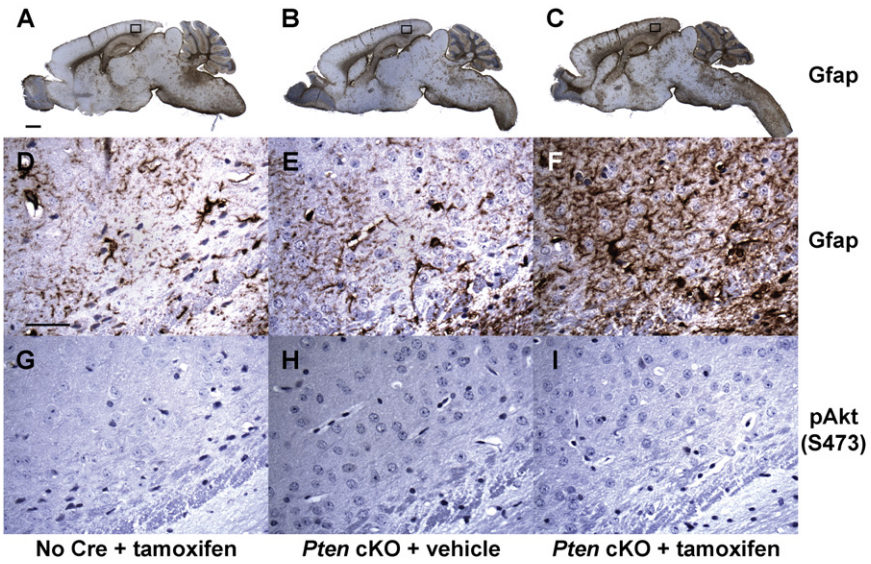

Figure 1. *Pten* Deletion in Adult Astrocytes Does Not Disrupt Brain Architecture or Activate Akt

(A–C) Sagittal sections were immunostained for Gfap (brown) and counterstained with hematoxylin. Magnified views of boxed regions for Gfap IHC (D–F) and pAkt S473 IHC (G–I, brown) are shown.

(A, D, and G) *Pten*$^{loxP/loxP}$ mouse injected with tamoxifen. (B, E, and H) *CreER*; *Pten*$^{loxP/loxP}$ mouse injected with vehicle.

(C, F and I) *CreER*; *Pten*$^{loxP/loxP}$ mouse injected with tamoxifen.

Scale bar in (A) is 1 mm and applies to (A)–(C). Scale bar in (D) is 50 μm and applies to (D)–(I). See also Figure S1.

such as the corpus callosum and internal capsule (Figures S3C–S3H, arrows). These cells were highly proliferative (Figures S3F–S3H and insets) and Pten null (Figure S3K, arrow). They may represent early stages of tumor growth or indicate cells in transit toward distant sites. Significantly, 22% (14/63) of tumors developed in sites independent of proliferative niches, including the cerebellum, spinal cord, or the ventral brain stem (Figures 3G–3I), in the absence of any other microscopically detectable tumor or abnormally proliferating cells in the brain including the progenitor niches, eliminating the possibility that they arose by spread from a distant established tumor mass. Although it is possible that tumor-initiating cells originating from progenitor-rich regions populated these tumors, we also identified early lesions and hyperproliferative cells in the cerebellum of brains where no aberrant proliferation in progenitor niches was apparent (Figures S3I and S3J, and inset).

Common RTK Amplification and Overexpression in *Pten*; *p53* cKO Mouse HGA

Array comparative genomic hybridization (aCGH) analysis revealed that most tumors carried multiple focal amplifications (CN >3) and deletions (CN <1.5), large-scale CN gains and losses, and more complex patterns of chromosomal copy number alterations (CNAs). The most frequent focal amplification, present in 24% (12/50) of tumors (ten of these with CN >3), was localized to Chr6A2 and included *Met* (Figure 4A), which encodes an RTK amplified in human glioblastomas, as well as other genes, some with association to HGG (Table S1). Additional focal amplifications involved *Egfr* and *Pdgfra*, encoding two RTKs that have been strongly implicated in the pathogenesis of HGG (Furnari et al., 2007). The region including *Egfr* was focally amplified in four tumors (Figure S4A), whereas the majority of Chr11 containing *Egfr* was amplified to a high degree in an additional tumor. Reverse transcription (RT)-PCR of *Egfr* transcripts from tumors with or without amplification did not detect truncations analogous to the *EGFR vIII* mutated variant found in some human glioblastomas (data not shown). The *Pdgfra* gene was contained within regions of high-level focal amplification in two tumors, and regions of focal gain (CN ranging from 2.3 to 3) in an additional five tumors (Figure S4B). All except one of the *Pdgfra* amplicons included the gene encoding the RTK Kit. Large-scale gains of Chr5, including *Pdgfra*, were found in an additional nine tumors. Most of the amplifications and gains of the three RTK genes described were mutually exclusive, although three tumors had concurrent focal amplifications of *Met* and another RTK. Thus, 40% (20/50) of *Pten*; *p53* cKO tumors contained somatic focal CNAs in these three RTK genes.

Gene amplification was confirmed by fluorescence in situ hybridization (FISH) (Figures 4A; Figures S4A and S4B). Real-time RT-PCR showed that focal amplification was consistently associated with high expression levels of the targeted RTK (Figure S4C). Several HGAs overexpressed RTKs, most frequently *Pdgfra*, in the absence of a detectable gene amplification event, as has been observed in human astrocytomas (Furnari et al., 2007). Western blot analysis showed that Met (lanes 7–9) and Egfr (lanes 3 and 5) overexpression in HGG was correlated with gene amplification, whereas Pdgfr-α was overexpressed in the majority of HGA samples and did not correlate with CN (Figure 4B). As expected for Pten-deficient tumors, levels of pAkt were elevated compared to normal cortex (Figures 3A and 4B). Interestingly, levels of pMapk T202/Y204 were not consistently altered among tumor samples, suggesting that steady-state signaling through the Ras/Mapk pathway was not necessarily elevated in HGA. There was no consistent correlation between RTK overexpression and tumor histology, or with levels of pMapk T202/Y204. Levels of pS6 S235/236 were more variable and tended to correlate with total S6 protein levels (Figure 4B).

Rb1 Deletion Further Contributed to Tumor Formation in cKO Mice

To model the concurrent dysregulation of the RTK/PI3K/AKT, p53, and RB pathways found in the majority of HGGs (Cerami et al., 2010; Cancer Genome Atlas Research Network, 2008; Parsons et al., 2008), we generated *CreER*; *Pten*$^{loxP/loxP}$; *Tp53*$^{loxP/loxP}$; *Rb1*$^{loxP/loxP}$ compound mice (hereafter termed triple cKO mice) and induced Cre activity as described above. Deletion of *Rb1* in addition to *Pten* and *Tp53* significantly reduced the latency of tumor development and time to morbidity

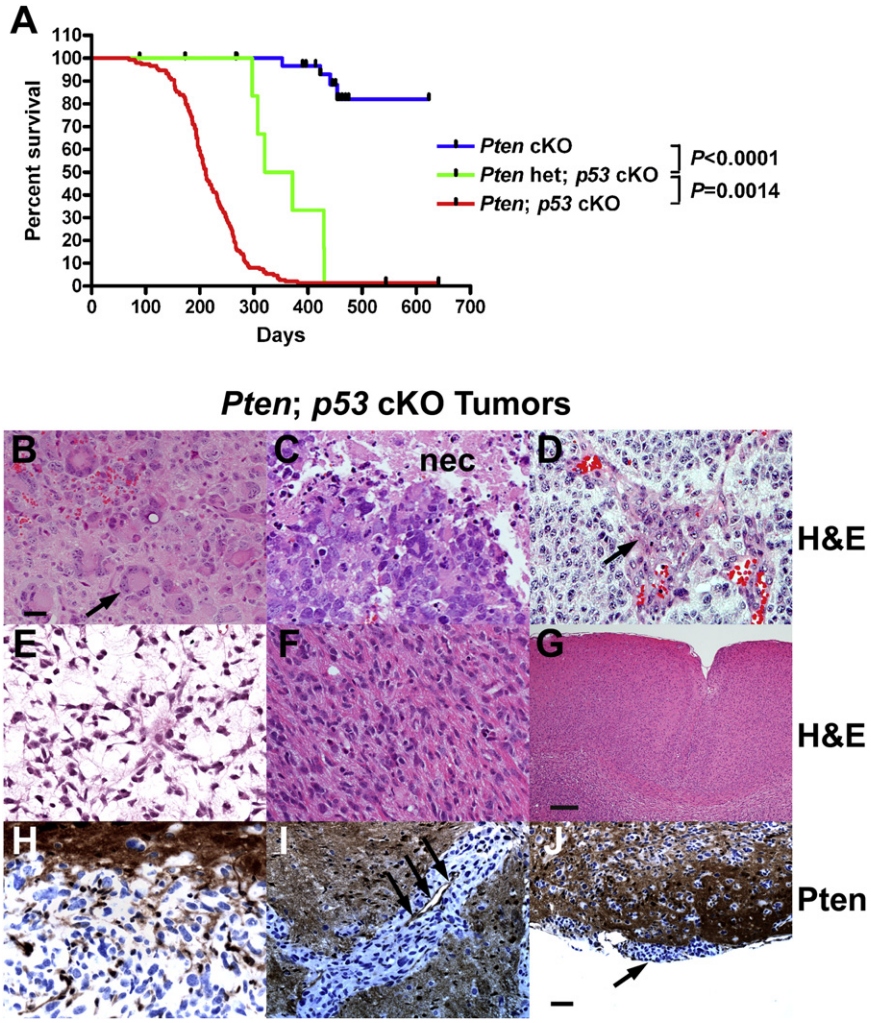

Figure 2. HGAs Arising from *Pten*; *p53* cKO Mice

(A) Kaplan-Meier survival analysis on tamoxifen-induced cohorts consisting of *Pten* cKO (n = 34; blue), *Pten*$^{loxP/+}$; *p53* cKO (n = 6; green), and *Pten*; *p53* cKO mice (n = 148; red).

(B–G) H&E of *Pten*; *p53* cKO brains showing recurrent histological features: glioblastoma with multinucleated giant cell phenotype (B, arrow), necrotic foci (C, nec) and sometimes microvascular proliferation (D, arrow), and anaplastic astrocytoma with myxoid degeneration (E) and diffusely infiltrating tumor cells (F) sometimes consistent with gliomatosis (G).

(H–J) IHC for Pten (brown) counterstained with hematoxylin highlighting areas of perivascular invasion (I) and leptomeningeal spread (J). Arrows in (I) indicate a blood vessel, whereas the arrow in (J) points to the pial membrane overlying tumor cells. Scale bar in (B) is 20 μm and applies to (B)–(F) and (H). Scale bar in (G) is 200 μm. Scale bar in (J) is 50 μm and applies to (I) and (J).

See also Figure S2.

from a median of 211 days to 159 days (Figure 5A). Of triple cKO brains, 85% (26/31) contained HGAs encompassing the same histological variation observed in *Pten*; *p53* cKO mice (Figure 5B; data not shown). Deletion of *Pten* in tumors was confirmed by IHC (Figure 5C), and deletion of *Tp53* and *Rb1* was demonstrated by PCR (Figures S5A and S5B). Triple cKO and *Pten*; *p53* cKO tumors showed similar high proliferation rates (Figures 5D; Figure S5C), invasive properties and immunophenotypes (data not shown), and pathway activation, with consistently elevated pAkt at S473 and T308 and variable pS6 S235/236 and p-Mapk (Figure 6).

aCGH showed a significant difference in the selective pressure for amplifications with no focal amplifications of the RTKs *Met* and *Egfr* in triple cKO tumors compared to 30% of *Pten*; *p53* cKO tumors showing focal amplification of one or both of these genes (p = 0.003). Large-scale gains of the Chrs containing these genes were also not consistently associated with RTK overexpression in triple cKO tumors (Figure 6). However, the frequency of *Pdgfra* amplification was very similar between *Pten*; *p53* cKO tumors and triple cKO tumors (14% in both; p = 1), and both sets of tumors showed frequent overexpression of Pdgfra, even in the absence of focal amplification (Figures 4 and 6). Thus, *Rb1* inactivation further cooperated with *Pten* and *Tp53* deletions to generate HGAs with similar histopathological and biochemical signatures, but different selective pressure for RTK amplifications.

Similar CNAs in cKO Mouse Tumors and Human HGA

In addition to genes encoding the RTKs mentioned previously, other notable genes contained within regions of CNA included amplification of *Cdk4*, *Cdk6*, *Ccnd1*, *Ccnd2*, and *Ccnd3*, which directly regulate Rb activity at the G_1/S cell cycle checkpoint, as well as loss of *Dcc* and *Smad4*. Expression changes in all of these genes have been implicated in glioma biology (Buschges et al., 1999; Kjellman et al., 2000; Cancer Genome Atlas Research Network, 2008; Reyes-Mugica et al., 1997). Of 50 *Pten*; *p53* cKO tumors, 12 (24%) had an amplification or deletion in at least one gene that would be expected to promote progression through the cell cycle (Table S2). Analysis of Rb null tumors showed that three of 21 tumors (14%) also had focal mutations in key cell cycle regulatory genes (p = 0.5), although these did not involve the upstream regulators of Rb (Table S2). We observed large deletions of Chr14 that included the *Rb1* locus in four of 50 *Pten*; *p53* cKO tumors (8%); however, similar deletions of Chr14 were also detected in six of 21 triple cKO tumors (29%), suggesting that *Rb1* was not the critical gene targeted by these deletions. Finally, *Mycn*, which has been proposed to promote cell cycle progression in the context of tumorigenesis (Pession and Tonelli, 2005), was amplified or gained in five (10%) *Pten*; *p53* and four (19%) triple cKO tumors (Figure S6A). Thus, the data support the notion that dysregulation of cell cycle regulation through additional mutations provides additional selective advantages above that provided by *Rb1* loss alone.

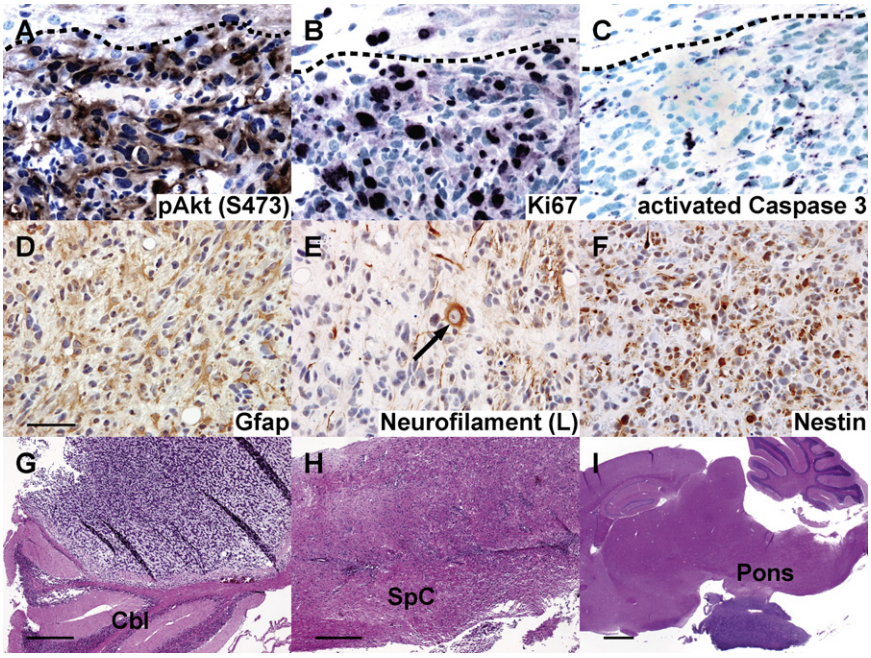

Figure 3. Immunophenotype of *Pten*; *p53* cKO HGAs

(A–C) Sections from a brain containing anaplastic astrocytoma were immunostained for pAkt S473 (A, brown), Ki67 (B, purple), and active Caspase-3 (C, purple), counterstained with hematoxylin (A) or methyl green (B and C). The dashed line indicates the approximate interface between normal cerebral cortex above and tumor below.

(D–F) IHC (brown) of anaplastic astrocytoma for Gfap (D), the light chain of Neurofilament (E), and Nestin (F), counterstained with hematoxylin. The arrow in (E) indicates the soma of a neuron.

(G–I) H&E showing tumors in the cerebellum (Cbl), spinal cord (SpC), and growing as an exophytic mass from the pons. Scale bar in (D) is 50 μm and applies to (A)–(F). Scale bars in (G) and (H) are 200 μm. Scale bar in (I) is 1 mm.

See also Figure S3.

Overall, large-scale CNAs were well conserved between the two models (Figure 7). The region of Chr12 that is deleted in 54% of *Pten*; *p53* and 52% of triple cKO tumors shares synteny with human Chr14q, which is lost in ~25% of glioblastomas. Similarly, partial loss of Chr14, occurring in 20% of *Pten*; *p53* and 43% of triple cKO tumors (p = 0.08), is syntenic to both human Chr14q and 13q, which undergo LOH in ~30% of glioblastomas. In fact, with the exception of Chr10q (which contains the *PTEN* locus), Chr14q and 13q losses are among the most frequent in glioblastoma (Cancer Genome Atlas Research Network, 2008; Parsons et al., 2008). Other significant large CNAs occurring in both models include loss of Chr9 and Chr18 and gain of Chr3, whereas partial deletion of Chr16 was more common in *Pten*; *p53* cKO tumors (p = 0.003). One of the more frequent focal deletions noted in triple but not in *Pten*; *p53* cKO tumors involves *Lrp1b*, which was lost in 43% (nine of 21) of tumors (Figure S6B), including six intragenic deletions. *LRP1B* deletions, including intragenic deletions, have been reported in glioblastoma (Parsons et al., 2008; Paugh et al., 2010; Yin et al., 2009; Zarghooni et al., 2010) as well as other tumor types (Cengiz et al., 2007; Langbein et al., 2002; Nagayama et al., 2007; Nakagawa et al., 2006; Sonoda et al., 2004). Taken together, the genomic landscapes of tumors arising from these murine HGA models are similar to each other and, more importantly, resemble human glioblastomas.

Gene Expression Signatures from Mouse HGAs Significantly Resemble Human Disease

Gene expression profiles were analyzed for 24 *Pten*; *p53* and 14 triple cKO HGAs. Unsupervised hierarchical clustering segregated the tumors into three distinct subgroups (Figure 8A; hierarchical cluster [HC] 1–HC3). Tumors from each cKO background were present in all three subgroups, further demonstrating that similar HGAs arise despite differences in the number of initiating mutations. Grade III anaplastic astrocytomas or pilomyxoid tumors did not cluster with specific subgroups; however, glioblastomas were exclusively found in HC2 and 3, not in HC1 (p = 0.0001). Notably, 38% (11/29) of HC1 and HC2 tumors, and none of the HC3 tumors, had focal amplifications in RTK genes (p = 0.04; Figure 8A). Several studies have identified gene expression subgroups in human HGG. Using gene set enrichment analysis (GSEA), we demonstrated highly significant similarity among the expression signatures of the mouse HC1, HC2, and HC3 subgroups with the human HGG expression subgroups that were identified by comparing prognosis, termed Proneural, Proliferative, and Mesenchymal, respectively (Phillips et al., 2006) (Figure 8B; Table S3). The Cancer Genome Atlas Project (TCGA) identified four expression subgroups that correlate to some extent with specific combinations of mutations (Verhaak et al., 2010), and there was also significant similarity between signatures in mouse HC1, with the TCGA Proneural and Neural subgroups, HC2 with the Proneural subgroup, and HC3 with the Mesenchymal subgroup (Table S3). Single-sample GSEA was also used to demonstrate the correlation of each individual mouse tumor gene expression profile with the gene sets for each human subgroup (Figure 8C). Interestingly, 78% (seven of nine) of the mouse HC3 tumors were exophytic tumors arising from the basal hypothalamus or the ventral pons (Figures 3I and 8A). To determine if this location was strongly associated with a specific expression signature in human tumors from similar locations, we analyzed the gene expression signatures of six human exophytic gliomas arising from the brain stem along with published data from pediatric HGG (Paugh et al., 2010) and adult glioblastoma (Lee et al., 2008). Single-sample GSEA showed heterogeneity among the human exophytic brain stem gliomas, with 33% (two of six) showing significant similarity to the Mesenchymal subclass, whereas 67% (four of six) showed the most significant similarity to the Proneural subclass (Figure S7). Similarly, we found gene expression signature heterogeneity among 31 grade IV human diffuse intrinsic pontine gliomas, with a similar proportion showing significant similarity to the

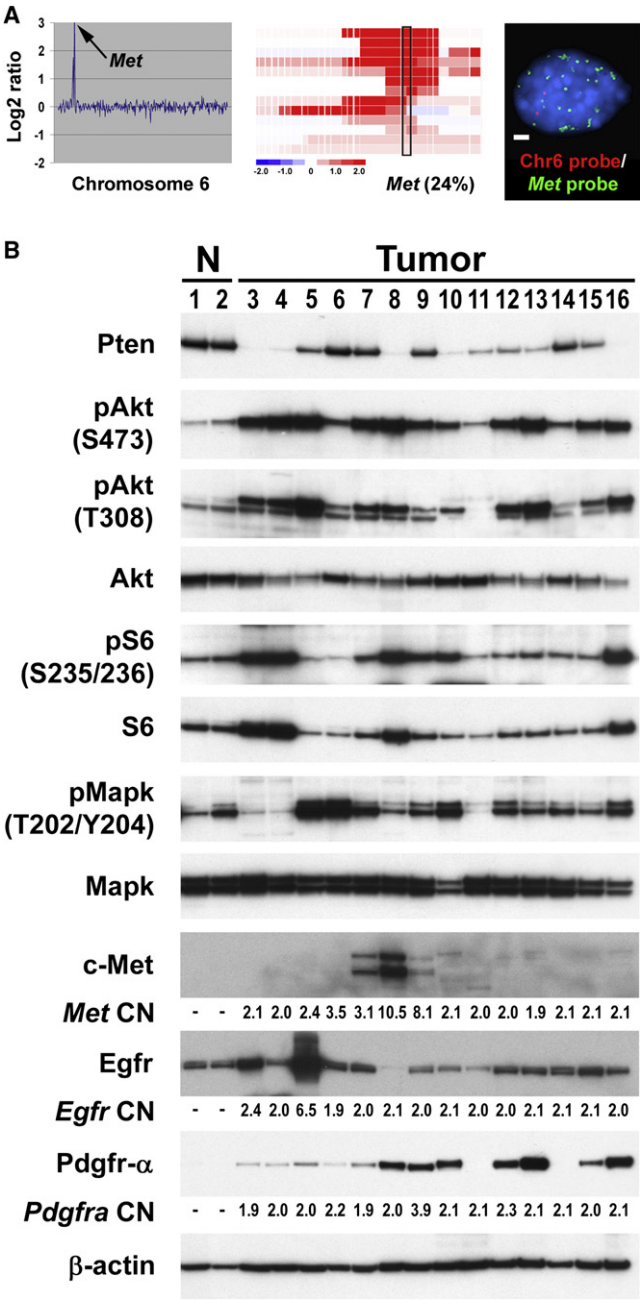

Figure 4. Focal Amplification, Signaling Pathway Activation, and Overexpression of RTKs in *Pten*; *p53* cKO HGA

(A) Recurrent focal amplification of *Met* in *Pten*; *p53* cKO HGA. aCGH plot of Chr6 location on the x axis and $\log_2$ ratio on the y axis is shown for a representative tumor (left panel). Amplified region containing *Met* is indicated. The middle panel is a heat map of $\log_2$ ratio showing focal CN gains in 13 tumors (horizontal bars) in the amplified region surrounding *Met*. The boxed region contains *Met*. Color scale with corresponding $\log_2$ ratio value is below. The right panel illustrates FISH on same tumor as left panel showing amplification of *Met* (green) compared to control Chr6 probe (red). Scale bar is 2 μm.

(B) Survey of pathway activation and RTK expression in *Pten*; *p53* cKO HGAs. Lysates from *Pten; p53* cKO mice were prepared from cortex that was grossly free of tumor (lanes 1 and 2) or from HGAs demonstrating a variety of histological features (lanes 3–16) and analyzed by western blots with the indicated antibodies. The *Met*, *Egfr*, and *Pdgfra* gene CNs below the corresponding blots are calculated from $\log_2$ ratio values obtained from aCGH on the same tumor sample.

See also Figure S4, and Tables S1 and S2.

Mesenchymal subgroup (unpublished data). Thus, the Mesenchymal signature found in the majority of mouse exophytic tumors arising from the brain stem or basal hypothalamus was also found in a subset of human gliomas arising from the brain stem.

Tp53 Loss Was Required for Gliomagenesis

To examine the cooperativity between tumor suppressors in the triple cKO mice, *Pten*; *Rb1* cKO and *p53*; *Rb1* cKO mice were also evaluated. No brain tumors were detected in 38 *Pten*; *Rb1* cKO brains that were serially sectioned in their entirety, although eight had pituitary tumors, which have been noted in *Rb1*$^{+/-}$ mice. Of 19 *Rb1*; *p53* cKO mice, 13 (68%) developed brain tumors with prolonged latency compared to *Pten*; *p53* cKO mice (Figure S5D). Two of these mice had tumors of morphology consistent with primitive neuroectodermal (PNET), although they did not show robust synaptophysin staining. An additional three mice had tumors within the olfactory bulb with strong resemblance to human olfactory neuroblastoma. Ten of 13 mice with brain tumors had HGA with histopathological features comparable to tumors from the other models (Figures S5E–S5G; data not shown). All but one of the tumors maintained Pten expression (Figures S5H–S5J). However, pAkt expression was strong throughout seven of 13 tumors (54%) (Figures S5K and S5L), and showed patchy or lower-level staining in an additional three tumors, indicating that the PI3K/AKT pathway is engaged in the majority of *Rb1*; *p53* cKO tumors.

DISCUSSION

Tumor Suppressor Cooperativity in Astrocytoma

Induced gene deletion in the adult brain reveals selective cooperativity among key tumor suppressors in the developmental context where the majority of HGAs arise. The high penetrance of HGA in mice with induced combined mutation of *Pten*, *Tp53*, and *Rb1* shows that the same core pathways drive gliomagenesis in mouse and human. The mutation spectrum in human glioblastomas has been extensively studied. More than 90% of human glioblastomas are primary glioblastomas that arise de novo without clinical or histological evidence of progression from a preexisting lesion (Louis et al., 2007). In the absence of clear progression, there is no unambiguous indication whether specific frequent genetic mutations arise preferentially as early or late events. This timing is implied by the analysis of tumor progression for the less-common secondary glioblastomas that arise as a consequence of malignant transformation from low-grade diffuse astrocytomas. However, there are distinct differences in the molecular pathogenesis of primary and secondary glioblastomas. Most significantly, *IDH1* mutations occur in more than 70% of secondary glioblastomas and the lower-grade lesions from which they arise but are rare in primary glioblastomas (Yan et al., 2009). This suggests that primary glioblastomas lack a common initiating mutation found in secondary

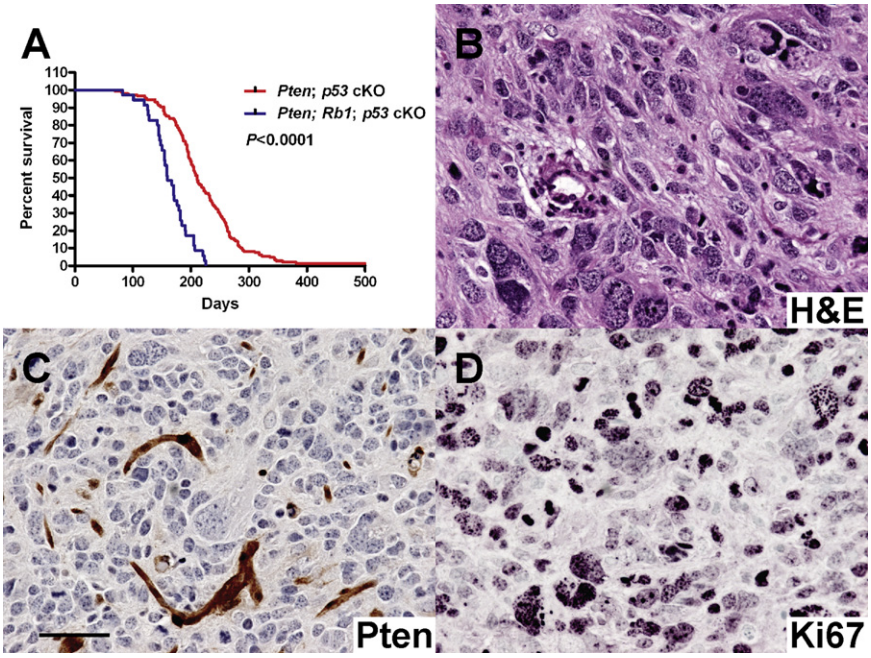

Figure 5. HGAs Arising from Triple cKO Mice

(A) Kaplan-Meier survival analysis was performed on tamoxifen-induced cohorts consisting of *Pten*; *p53* (n = 148; red) and triple cKO mice (n = 35; blue).

(B) H&E of a triple cKO brain containing a giant cell glioblastoma.

(C) IHC for Pten (brown) on a section corresponding to the same tumor counterstained with hematoxylin.

(D) IHC for Ki67 (purple) on an adjacent section counterstained with methyl green. Scale bar in (C) is 50 μm and applies to (B)–(D).

See also Figure S5.

glioblastoma, and may be driven by alternative initiating events. Thus, the role of common mutations in primary glioblastoma to act as initiating or late events remains unclear.

Using mouse models, we induced mutations in specific key tumor suppressors and evaluated which mutations cooperated to cause glioma, and which additional mutations provided a selective advantage. In our models none of these tumor suppressor deletions alone induced astrocytomas with high frequency, although *Tp53* deletion induced late onset, low-frequency astrocytomas similar to a previous study (Zheng et al., 2008) (data not shown). The greatest cooperativity and earliest tumor onset occurred with simultaneous mutation of all three tumor suppressors, consistent with concurrent mutations in these three pathways occurring in virtually all human glioblastomas. Combinations of mutations that included *Tp53* induced astrocytomas efficiently. This supports a role for *Tp53* inactivation in astrocytoma initiation and is consistent with the high frequency of *TP53* mutations and low frequency of *RB1* and *PTEN* mutations in grade II human astrocytomas (Louis et al., 2007; Wen and Kesari, 2008). The significantly earlier onset of tumors arising from *Pten*; *p53* deletion compared to *Rb1*; *p53* deletion demonstrated that *Pten* loss cooperated more effectively than *Rb1* deletion with *p53* mutation. Importantly, we failed to detect any brain tumors arising from mice with targeted codeletions in *Rb1* and *Pten*. This does not necessarily indicate that these two pathways fail to cooperate in gliomas but, rather, indicates that the specific mutation of *Pten* and *Rb1* does not effectively cooperate in the absence of other mutations. In another study, expression of a truncated SV40 T antigen that inactivates all Rb family members induced mouse astrocytomas and cooperated with *Pten* loss (Xiao et al., 2005). This suggests that inactivation of all Rb family members may be required to initiate gliomagenesis or that the truncated T antigen exerted additional Rb-independent effects.

PTEN functions primarily by regulating RTK/PI3K/AKT signaling through its lipid phosphatase activity. Loss of Pten in several cell types within the brain during development, including neurons, astrocytes, and neural progenitor cells, has been shown to result in Akt activation and proliferation, but not tumorigenesis (Fraser et al., 2004; Gregorian et al., 2009; Groszer et al., 2001; Kwon et al., 2001). We found that Pten loss in the mature astrocyte induced elevated Gfap expression but did not demonstrate features of severe astrocytic gliosis, such as hypertrophy, hyperproliferation, and abnormal multinucleated astrocytes. Thus, Pten loss may disrupt cellular homeostasis enough to be detected as a cellular stress inducing a low-level astrogliosis response, but it is insufficient to drive proliferation, consistent with the inability to initiate gliomagenesis in the absence of other mutations. Importantly, Pten loss did not substantially stimulate PI3K signaling, suggesting that in this context, basal signaling through the RTK/PI3K axis is not sufficient to elevate pathway activity, even in the absence of negative regulation. This is consistent with the cell type-specific feedback regulation that inhibits PI3K signaling in glia, but not in neurons (Chalhoub et al., 2009). Therefore, the net outcome of mutations that deregulate PI3K signaling depends on the cellular and developmental context.

Site of Astrocytoma Development

To precisely define a cell of origin for a tumor in a model system, it is necessary to use highly selective methods to induce gene mutations only in specific populations of cells. Using this approach, several recent reports identified neural progenitor cells as the likely cell of origin for HGAs in mouse models and showed that cells outside of the proliferative niche failed to form HGAs with combinations of deletion in *Pten*, *Tp53*, *Nf1*, and *Rb1* (Alcantara Llaguno et al., 2009; Holland et al., 2000; Jacques et al., 2010; Wang et al., 2009). In contrast, the goal of this study was to induce widespread tumor suppressor deletion in astrocytes and progenitor cells in the adult brain to test the ability of these mutations to induce gliomas in diverse brain regions. Using *GFAP-CreER* mice, we induced Cre activity in a much larger population of cells outside of proliferative niches than within the neurogenic zones of adult brain. We found

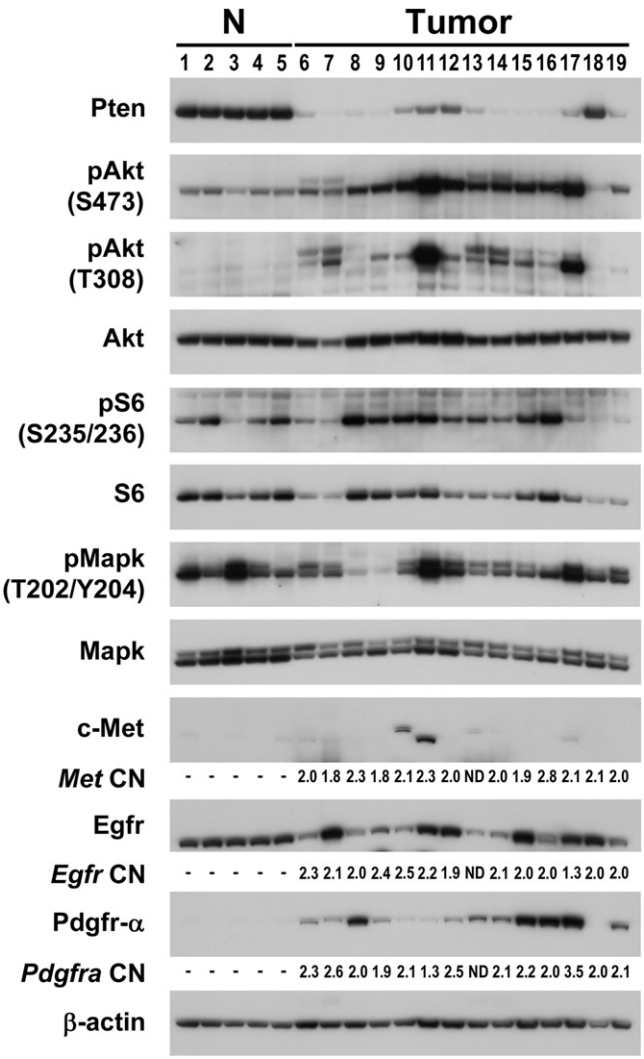

Figure 6. Signaling Pathway Activation in Triple cKO Mice

Lysates from triple cKO mice were prepared from cortex that was grossly free of tumor (lanes 1–5) or from HGAs demonstrating a variety of histological features (lanes 6–19) and analyzed by western blots with the indicated antibodies. The *Met*, *Egfr*, and *Pdgfra* gene CNs below the corresponding blots are calculated from $\log_2$ ratio values obtained from aCGH on the same tumor sample. One tumor sample (lane 13) did not have a corresponding aCGH profile (ND).

HGAs both within and outside of proliferative niches, and heterogeneity in tumor histopathology was independent of location. Human glioblastomas also often occur in regions not associated with neurogenesis. Our analysis may underestimate the frequency of tumors arising outside of the neurogenic niche because we evaluated tumors at the time of morbidity, where large tumors that may have arisen in surrounding regions and grown into the neurogenic niche were scored as associated with proliferative zones. The higher frequency of tumors arising in association with proliferative niches is consistent with progenitor/stem cells having a greater propensity for malignant transformation. Indeed, despite much lower Cre activity in neurogenic niches, tumors arose predominantly in areas contiguous with or adjacent to neural stem cell niches in the brain, and we also detected early invasion of proliferative tumor cells through white matter tracts in these regions (Figures S3C–S3H). Nevertheless, macroscopic HGAs and microscopic proliferative lesions were also found in areas isolated from canonical neural progenitors in mice without detectable hyperplasia or abnormalities in proliferative zones (Figures 3G–3I; Figures S3I, and S3J). Although the precise cell of origin remains to be determined, these tumors may arise from mature astrocytes (Dufour et al., 2009), locally resident progenitor cells (Laywell et al., 2000; Lee et al., 2005), or progenitor cells that escaped from proliferative niches to populate distant sites.

Recently, Jacques et al. (2010) reported that tumors arising from *p53*; *Rb1* or *Pten*; *p53*; *Rb1* codeletions induced in SVZ cells, presumably neural stem cells and/or progenitor cells, were almost exclusively of the PNET phenotype, whereas *Pten*; *p53* codeletion resulted in gliomas. In contrast, all of these combinations of tumor suppressor inactivation induced in adult mice by *GFAP-creER* gave rise to HGAs, consistent with concurrent mutation of these pathways in human HGAs. None of the tumors arising in triple cKO mice was a typical PNET on the basis of histopathological features, lack of synaptophysin expression, and the consistent expression of Gfap (data not shown). The discrepancies between tumor types obtained could be explained by differences in the specific cells targeted by adeno-Cre virus injections into the ventricle compared to *GFAP-CreER*, the age of the mice at the time of tumor suppressor inactivation, inflammation and wound healing secondary to the intracranial injection procedure, differences in genetic background, or differences in the *Pten* floxed strain used in the two studies.

Initiating Mutations Drive Selective Pressures for Additional Disruption within the Same Core Pathways

Genome-wide analysis of CNAs in mouse HGAs revealed strong selective pressure in *Pten*; *p53* cKO tumors for focal amplifications in the RTKs *Met*, *Egfr*, and *Pdgfra*, genes that are also well-known amplification targets in human glioblastoma (Furnari et al., 2007). These somatic amplifications in upstream components of PI3K signaling strongly suggest that *Pten* deletion alone was insufficient to activate the pathway to the levels required to drive gliomagenesis in this model and/or that pathways downstream of RTKs other than PI3K/Akt are required for HGA growth. Although RTKs are known to signal through both the Mapk and PI3K pathways, in the mouse HGAs, RTK amplifications were associated with consistently high PI3K signaling, but not consistently elevated Mapk signaling. This demonstrates that the downstream consequences of RTK activation vary in gliomas. Somatic mutations also demonstrated that amplifications of different RTKs were not equivalent. *Pdgfra* amplification and overexpression were very similar between *Pten*; *p53* cKO and triple cKO tumors; however, there were no amplifications of *Met* or *Egfr* in triple cKO tumors, where G_1 cell cycle checkpoint control was compromised by *Rb1* deletion. This implies that the initiating mutations may strongly influence the selective advantage of hyperactivation of specific RTKs. The more uniform involvement of *Pdgfra* indicates that it may play a unique role relative to other RTKs. Further investigation is needed to delineate the mechanisms driving different selective pressures for RTK amplifications in *Pten*; *p53* cKO and triple cKO tumors.

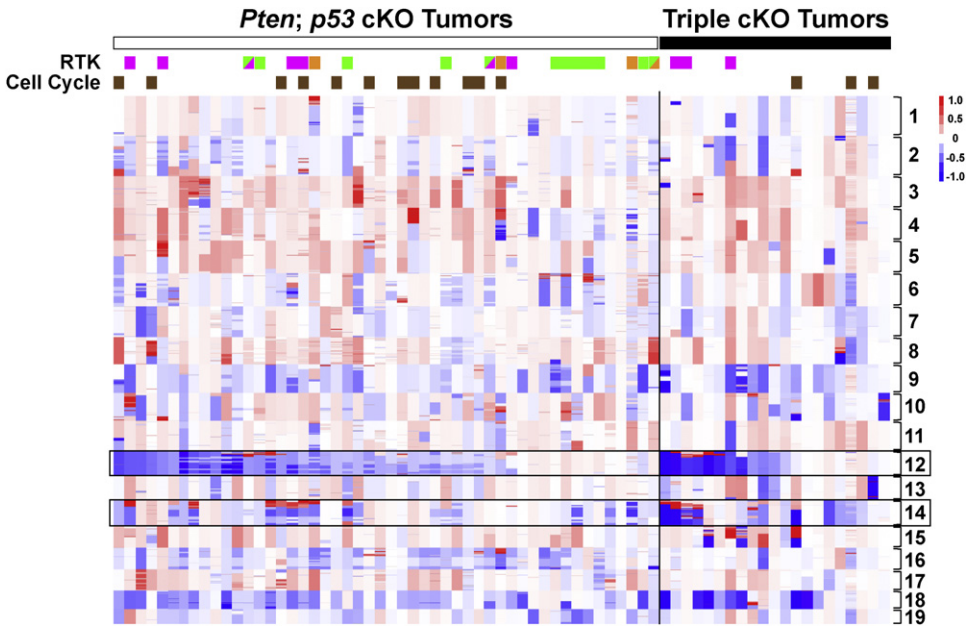

Figure 7. Genome-Wide CNAs in Murine HGAs

Heat map of genomic CN imbalances showing segmented $\log_2$ ratio from aCGH data to identify CN gains (red) and losses (blue) in 50 *Pten*; *p53* cKO (white bar) and 21 triple cKO (black bar) tumors. Amplifications and gains of genes encoding the RTKs Met (green bars), Egfr (orange bars), and Pdgfr-α (violet bars) are shown. Tumors with amplifications of the cell cycle-related genes shown in Table S2 are also indicated (brown bars). Chr numbers are indicated on the right, and frequent losses of Chr12 and Chr14 are boxed. Color scale with corresponding $\log_2$ ratio value is to the right. See also Figure S6.

Akt phosphorylation was also consistently elevated in *Rb1*; *p53* cKO tumors, showing a selective pressure for activation of PI3K signaling regardless of whether tumors were initiated by a mutation in this pathway.

Dysregulation of RB signaling leading to G_1/S progression appears to be a critical event in gliomagenesis. This pathway was also targeted by somatic amplifications, with *Pten*; *p53* cKO tumors showing amplification of Rb regulators as well as other cell cycle genes and triple cKO tumors showing amplification of pathway components downstream of Rb (Table S2). Again, we noted alterations in multiple pathway members in the same tumor, suggesting that pathway mutations cooperate to provide a greater selective advantage.

Relevance of the Mouse HGA Models to Human Disease

The murine HGAs reported here are relevant to human disease, reflecting a spectrum of tumor histology and molecular features. In addition to focal amplifications and deletions of known glioma genes, large-scale chromosomal losses in regions syntenic to those lost in human HGA were detected. Gene expression signatures from gliomas arising in *Pten*; *p53* or triple cKO mice fell into three subgroups showing significant similarity to the three expression subclasses of human high-grade glioma associated with tumor prognosis (Phillips et al., 2006). Importantly, tumor subgroups did not correlate with initiating mutations or tumor histology (Figure 8A). In humans the Mesenchymal subgroup is associated with the worse prognosis (Phillips et al., 2006). Unexpectedly, 78% (seven of nine) of the mouse tumors with greatest similarity to the Mesenchymal subgroup arose as exophytic tumors from the ventral base of the brain or the pons (Figure 8). Conversely, 78% (seven of nine) of tumors from this location had a Mesenchymal gene signature compared to 7% (two of 29) of HGAs in all other locations of the central nervous system ($p = 0.00009$), suggesting that the microenvironment or specific cells targeted in this region of brain contributed to tumor phenotype. Taken together, the somatically acquired genomic imbalances and the gene expression signatures of HGAs in *Pten*; *p53* cKO and triple cKO mice indicate that similar selective pressures drive gliomagenesis and generate similar tumors in humans and these mouse models, suggesting that they should be valuable for preclinical testing.

EXPERIMENTAL PROCEDURES

Mice

Mice were maintained on a predominantly FVB/NJ background with contributions from 129/SV and C57Bl6. The *GFAP-CreER*^{TM}A (FVB/NJ background) and floxed *Pten* (backcrossed six generations to FVB/NJ) mouse lines have been previously described (Chow et al., 2008; Suzuki et al., 2001) and were crossed to generate *GFAP-CreER*; *Pten*$^{loxP/loxP}$ mice. Controls were *Pten*$^{loxP/loxP}$ mice injected with tamoxifen, or *CreER*; *Pten*$^{loxP/loxP}$ mice injected with vehicle. Floxed *Tp53* and *Rb1* mice were obtained from the Mouse Models of Human Cancer Consortium repository (Jonkers et al., 2001; Marino et al., 2000). All combinations of compound floxed mice were generated by crossing *GFAP-CreER*; *Pten*$^{loxP/loxP}$ with *Tp53*; *Rb1* double-floxed mice. Tamoxifen (Sigma-Aldrich, St. Louis. MO, USA) was dissolved in corn oil (Sigma-Aldrich) at a concentration of 20 mg/ml at 37°C, filter sterilized, and stored for up to 7 days at 4°C in the dark. A 27G needle tuberculin syringe (Becton Dickinson, Franklin Lakes, NJ, USA) was used for intraperitoneal injections. Tamoxifen (9 mg/40 g body weight) was administered daily for 3 days after P28 (range P25–P49). There was no significant difference associated with the age of induction in the time from tamoxifen administration to tumor onset, or in the histology of the resulting tumors. Procedures for all mouse experiments were reviewed and approved by the Animal Care and Use Committee at St. Jude Children's Research Hospital, and are in compliance with national and

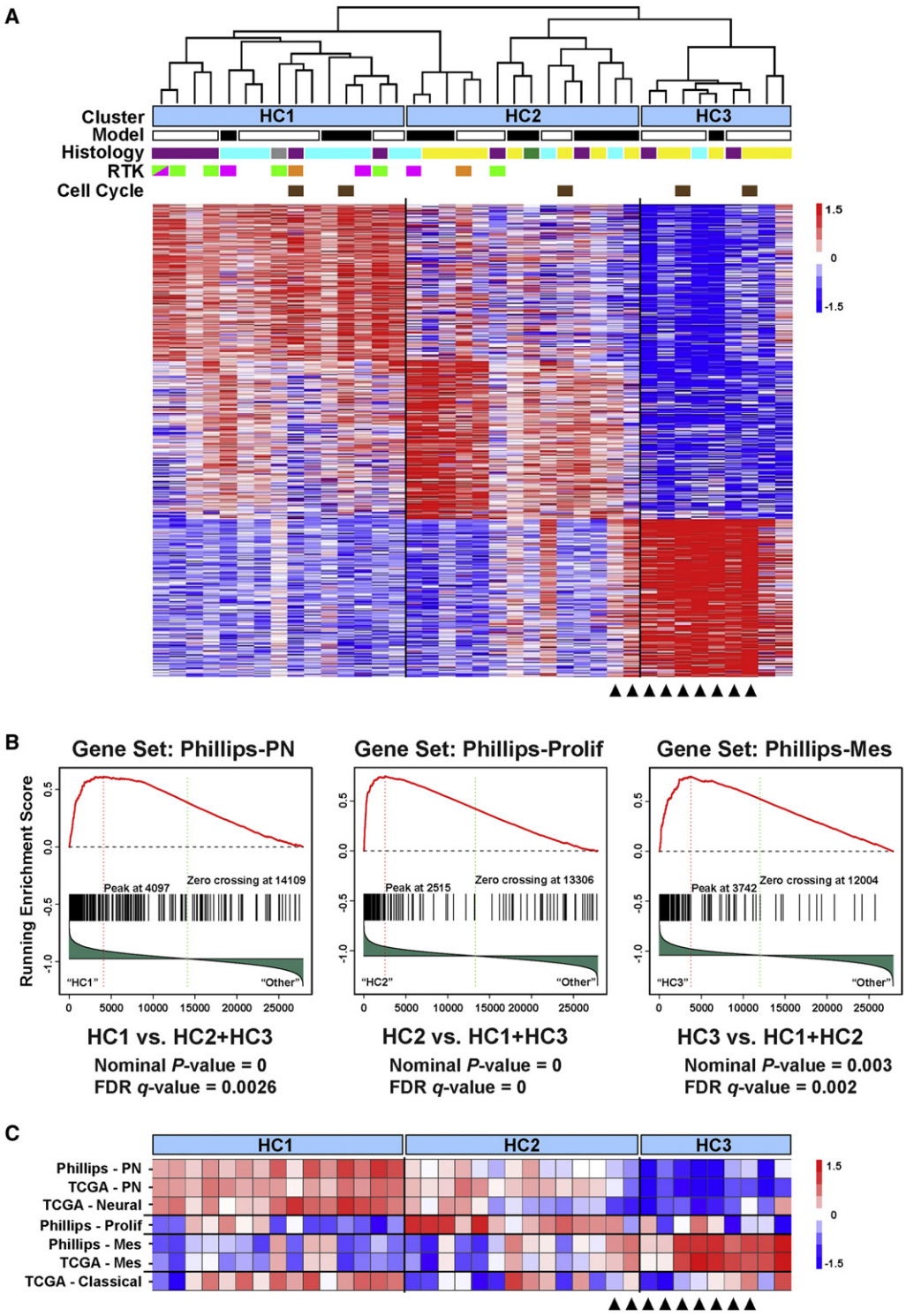

Figure 8. Gene Expression Signatures of Mouse HGAs Are Similar to Human Gene Expression Subgroups

(A) Gene expression profiles generated from *Pten*; *p53* cKO (Model: white bars) and triple cKO (Model: black bars) HGAs were analyzed by unsupervised hierarchical clustering using the top 1000 probe sets showing the greatest differential expression levels as selected by median absolute deviation scores. Three primary clusters were identified, HC1–HC3, and the dendrogram is shown on top. The heat map shows the most upregulated probe sets for each cluster derived using linear models algorithm. The primary histological features (Histology) are glioblastoma (yellow bars), HGA with myxoid degeneration (light-blue bars), anaplastic astrocytoma (purple bars), anaplastic oligoastrocytoma (dark-green bar), and one tumor (gray bar), which was not determined. Tumors with RTK and cell cycle-related gene mutations are indicated as in Figure 6. Tumors located at the base of the brain are marked with arrowheads. Color scale with corresponding Z-score values is to the right.

institutional guidelines. Mice were monitored daily and euthanized following NIH guidelines.

Mouse Tissue Collection

Mice were perfused with 1× phosphate-buffered saline (PBS) to exsanguinate tissues. Following dissection, half the brain containing a portion of the tumor, if evident, was fixed by immersion in 4% paraformaldehyde (PFA) in 1× PBS at 4°C overnight. If no tumor could be visually identified, the brain was divided sagittally, and both halves were fixed in this manner. The tissue was processed, embedded in paraffin, and 5 μm sections were cut. If the presence of a tumor was evident, several slides spanning the tumor were stained with H&E; if a tumor was not grossly apparent, every fifth slide was stained spanning the entire brain. All slides were examined by L.M.L.C., and sections containing tumor or other anomalies were viewed by S.J.B. and assigned diagnoses by D.W.E., a clinical neuropathologist. The second half of the tumor-containing brains was further dissected to separate tumor tissue from normal cortex. Several tubes of each if possible were immediately flash frozen on dry ice pellets for subsequent nucleic acid and/or protein preparations.

Mouse Tumor Analyses

Tumor diagnoses were assigned by D.W.E., a neuropathologist. Microarray analyses were performed using Roswell Park Cancer Institute (RPCI) 6.5K mouse BAC array, and Agilent mouse 244K Oligo array for array CGH, and Affymetrix Mouse Genome 430 2.0 chip for expression profiles.

Human Tumor Samples

Snap-frozen surgical samples of grade II exophytic brain stem gliomas or autopsy samples of normal brain stem were obtained from the St. Jude tumor bank. Histopathology was reviewed by D.W.E. These samples were collected and experiments performed with the informed consent of patients and/or their legal guardians under the approval of the St. Jude Children's Research Hospital Institutional Review Board.

Statistical Analysis

For categorical statistical analysis, we used two-sided Fisher's exact test.

ACCESSION NUMBERS

Array data is deposited in Gene Expression Omnibus (GEO) under accession number GSE22927.

SUPPLEMENTAL INFORMATION

Supplemental Information includes seven figures, three tables, and Supplemental Experimental Procedures and can be found with this article online at doi:10.1016/j.ccr.2011.01.039.

ACKNOWLEDGMENTS

We thank M. Dyer for providing mice, J.M. Lahti and V.A. Valentine from the Cancer Center Core Cytogenetics Laboratory for FISH analyses, the Hartwell Center for aCGH and gene expression microarray labeling, hybridization and data acquisition, M. Wang for help with aCGH data analysis, J. Mitchell and K. Cox for mouse genotyping, and A. Gajjar for support. L.M.L.C. was a recipient of the Jean-François St.-Denis Fellowship in Cancer Research from the Canadian Institutes of Health Research. This work was supported by grants to S.J.B. from the National Institutes of Health (CA135554 and CA096832), and by the Ryan McGee Foundation and ALSAC.

Received: July 14, 2010
Revised: November 23, 2010
Accepted: January 10, 2011
Published: March 14, 2011

REFERENCES

Alcantara Llaguno, S., Chen, J., Kwon, C.H., Jackson, E.L., Li, Y., Burns, D.K., Alvarez-Buylla, A., and Parada, L.F. (2009). Malignant astrocytomas originate from neural stem/progenitor cells in a somatic tumor suppressor mouse model. Cancer Cell *15*, 45–56.

Backman, S.A., Stambolic, V., Suzuki, A., Haight, J., Elia, A., Pretorius, J., Tsao, M.S., Shannon, P., Bolon, B., Ivy, G.O., and Mak, T.W. (2001). Deletion of Pten in mouse brain causes seizures, ataxia and defects in soma size resembling Lhermitte-Duclos disease. Nat. Genet. *29*, 396–403.

Brustle, O., and McKay, R.D. (1995). The neuroepithelial stem cell concept: implications for neuro-oncology. J. Neurooncol. *24*, 57–59.

Buschges, R., Weber, R.G., Actor, B., Lichter, P., Collins, V.P., and Reifenberger, G. (1999). Amplification and expression of cyclin D genes (CCND1, CCND2 and CCND3) in human malignant gliomas. Brain Pathol. *9*, 435–442.

Cancer Genome Atlas Research Network. (2008). Comprehensive genomic characterization defines human glioblastoma genes and core pathways. Nature *455*, 1061–1068.

Cengiz, B., Gunduz, M., Nagatsuka, H., Beder, L., Gunduz, E., Tamamura, R., Mahmut, N., Fukushima, K., Ali, M.A., Naomoto, Y., et al. (2007). Fine deletion mapping of chromosome 2q21-37 shows three preferentially deleted regions in oral cancer. Oral Oncol. *43*, 241–247.

Cerami, E., Demir, E., Schultz, N., Taylor, B.S., and Sander, C. (2010). Automated network analysis identifies core pathways in glioblastoma. PLoS ONE *5*, e8918.

Chalhoub, N., Zhu, G., Zhu, X., and Baker, S.J. (2009). Cell type specificity of PI3K signaling in Pdk1- and Pten-deficient brains. Genes Dev. *23*, 1619–1624.

Chow, L.M., and Baker, S.J. (2006). PTEN function in normal and neoplastic growth. Cancer Lett. *241*, 184–196.

Chow, L.M., Zhang, J., and Baker, S.J. (2008). Inducible Cre recombinase activity in mouse mature astrocytes and adult neural precursor cells. Transgenic Res. *17*, 919–928.

Dufour, C., Cadusseau, J., Varlet, P., Surena, A.L., de Faria, G.P., Dias-Morais, A., Auger, N., Leonard, N., Daudigeos, E., Dantas-Barbosa, C., et al. (2009). Astrocytes reverted to a neural progenitor-like state with transforming growth factor alpha are sensitized to cancerous transformation. Stem Cells *27*, 2373–2382.

Ferguson, K.L., Vanderluit, J.L., Hebert, J.M., McIntosh, W.C., Tibbo, E., MacLaurin, J.G., Park, D.S., Wallace, V.A., Vooijs, M., McConnell, S.K., and Slack, R.S. (2002). Telencephalon-specific Rb knockouts reveal enhanced neurogenesis, survival and abnormal cortical development. EMBO J. *21*, 3337–3346.

Fraser, M.M., Zhu, X., Kwon, C.H., Uhlmann, E.J., Gutmann, D.H., and Baker, S.J. (2004). Pten loss causes hypertrophy and increased proliferation of astrocytes in vivo. Cancer Res. *64*, 7773–7779.

Furnari, F.B., Fenton, T., Bachoo, R.M., Mukasa, A., Stommel, J.M., Stegh, A., Hahn, W.C., Ligon, K.L., Louis, D.N., Brennan, C., et al. (2007). Malignant astrocytic glioma: genetics, biology, and paths to treatment. Genes Dev. *21*, 2683–2710.

(B) GSEA enrichment plots. Each primary cluster was compared to the other two clusters using gene sets defining expression subgroups derived from human glioblastoma studies. The three gene sets from Phillips et al. (2006), i.e., Phillips-PN (Proneural), Phillips-Prolif (Proliferative), and Phillips-Mes (Mesenchymal), are the ones that are most significant for each cluster. The nominal p value and false discovery rate (FDR)-corrected q value are indicated below.
(C) Heat map of normalized enrichment scores calculated using single-sample GSEA comparing individual mouse tumors arranged by cluster as in (A) to gene sets defining expression subgroups previously identified in human glioblastoma. TCGA-PN, TCGA-Neural, TCGA-Classical, and TCGA-Mes are the four gene sets derived from Verhaak et al. (2010). Tumors located at the base of the brain are marked with arrowheads. Color scale with corresponding normalized enrichment score is to the right.
See also Figure S7 and Table S3.

Gregorian, C., Nakashima, J., Le Belle, J., Ohab, J., Kim, R., Liu, A., Smith, K.B., Groszer, M., Garcia, A.D., Sofroniew, M.V., et al. (2009). Pten deletion in adult neural stem/progenitor cells enhances constitutive neurogenesis. J. Neurosci. *29*, 1874–1886.

Groszer, M., Erickson, R., Scripture-Adams, D.D., Lesche, R., Trumpp, A., Zack, J.A., Kornblum, H.I., Liu, X., and Wu, H. (2001). Negative regulation of neural stem/progenitor cell proliferation by the Pten tumor suppressor gene in vivo. Science *294*, 2186–2189.

Holland, E.C., Celestino, J., Dai, C., Schaefer, L., Sawaya, R.E., and Fuller, G.N. (2000). Combined activation of Ras and Akt in neural progenitors induces glioblastoma formation in mice. Nat. Genet. *25*, 55–57.

Jacques, T.S., Swales, A., Brzozowski, M.J., Henriquez, N.V., Linehan, J.M., Mirzadeh, Z., O'Malley, C., Naumann, H., Alvarez-Buylla, A., and Brandner, S. (2010). Combinations of genetic mutations in the adult neural stem cell compartment determine brain tumour phenotypes. EMBO J. *29*, 222–235.

Jonkers, J., Meuwissen, R., van der Gulden, H., Peterse, H., van der Valk, M., and Berns, A. (2001). Synergistic tumor suppressor activity of BRCA2 and p53 in a conditional mouse model for breast cancer. Nat. Genet. *29*, 418–425.

Kjellman, C., Olofsson, S.P., Hansson, O., Von Schantz, T., Lindvall, M., Nilsson, I., Salford, L.G., Sjogren, H.O., and Widegren, B. (2000). Expression of TGF-beta isoforms, TGF-beta receptors, and SMAD molecules at different stages of human glioma. Int. J. Cancer *89*, 251–258.

Kwon, C.H., Zhu, X., Zhang, J., Knoop, L.L., Tharp, R., Smeyne, R.J., Eberhart, C.G., Burger, P.C., and Baker, S.J. (2001). Pten regulates neuronal soma size: a mouse model of Lhermitte-Duclos disease. Nat. Genet. *29*, 404–411.

Kwon, C.H., Zhao, D., Chen, J., Alcantara, S., Li, Y., Burns, D.K., Mason, R.P., Lee, E.Y., Wu, H., and Parada, L.F. (2008). Pten haploinsufficiency accelerates formation of high-grade astrocytomas. Cancer Res. *68*, 3286–3294.

Langbein, S., Szakacs, O., Wilhelm, M., Sukosd, F., Weber, S., Jauch, A., Lopez Beltran, A., Alken, P., Kalble, T., and Kovacs, G. (2002). Alteration of the LRP1B gene region is associated with high grade of urothelial cancer. Lab. Invest. *82*, 639–643.

Laywell, E.D., Rakic, P., Kukekov, V.G., Holland, E.C., and Steindler, D.A. (2000). Identification of a multipotent astrocytic stem cell in the immature and adult mouse brain. Proc. Natl. Acad. Sci. USA *97*, 13883–13888.

Lee, A., Kessler, J.D., Read, T.A., Kaiser, C., Corbeil, D., Huttner, W.B., Johnson, J.E., and Wechsler-Reya, R.J. (2005). Isolation of neural stem cells from the postnatal cerebellum. Nat. Neurosci. *8*, 723–729.

Lee, Y., Scheck, A.C., Cloughesy, T.F., Lai, A., Dong, J., Farooqi, H.K., Liau, L.M., Horvath, S., Mischel, P.S., and Nelson, S.F. (2008). Gene expression analysis of glioblastomas identifies the major molecular basis for the prognostic benefit of younger age. BMC Med. Genomics *1*, 52.

Louis, D.N., Ohgaki, H., Wiestler, O.D., and Cavenee, W.K., eds. (2007). WHO Classification of Tumours of the Central Nervous System, Fourth Edition (Lyon, France: International Agency for Research on Cancer).

MacPherson, D., Sage, J., Crowley, D., Trumpp, A., Bronson, R.T., and Jacks, T. (2003). Conditional mutation of Rb causes cell cycle defects without apoptosis in the central nervous system. Mol. Cell. Biol. *23*, 1044–1053.

Marino, S., Vooijs, M., van Der Gulden, H., Jonkers, J., and Berns, A. (2000). Induction of medulloblastomas in p53-null mutant mice by somatic inactivation of Rb in the external granular layer cells of the cerebellum. Genes Dev. *14*, 994–1004.

Marino, S., Krimpenfort, P., Leung, C., van der Korput, H.A., Trapman, J., Camenisch, I., Berns, A., and Brandner, S. (2002). PTEN is essential for cell migration but not for fate determination and tumourigenesis in the cerebellum. Development *129*, 3513–3522.

Nagayama, K., Kohno, T., Sato, M., Arai, Y., Minna, J.D., and Yokota, J. (2007). Homozygous deletion scanning of the lung cancer genome at a 100-kb resolution. Genes Chromosomes Cancer *46*, 1000–1010.

Nakagawa, T., Pimkhaokham, A., Suzuki, E., Omura, K., Inazawa, J., and Imoto, I. (2006). Genetic or epigenetic silencing of low density lipoprotein receptor-related protein 1B expression in oral squamous cell carcinoma. Cancer Sci. *97*, 1070–1074.

Parsons, D.W., Jones, S., Zhang, X., Lin, J.C., Leary, R.J., Angenendt, P., Mankoo, P., Carter, H., Siu, I.M., Gallia, G.L., et al. (2008). An integrated genomic analysis of human glioblastoma multiforme. Science *321*, 1807–1812.

Paugh, B.S., Qu, C., Jones, C., Liu, Z., Adamowicz-Brice, M., Zhang, J., Bax, D.A., Coyle, B., Barrow, J., Hargrave, D., et al. (2010). Integrated molecular genetic profiling of pediatric high-grade gliomas reveals key differences with the adult disease. J. Clin. Oncol. *28*, 3061–3068.

Pession, A., and Tonelli, R. (2005). The MYCN oncogene as a specific and selective drug target for peripheral and central nervous system tumors. Curr. Cancer Drug Targets *5*, 273–283.

Phillips, H.S., Kharbanda, S., Chen, R., Forrest, W.F., Soriano, R.H., Wu, T.D., Misra, A., Nigro, J.M., Colman, H., Soroceanu, L., et al. (2006). Molecular subclasses of high-grade glioma predict prognosis, delineate a pattern of disease progression, and resemble stages in neurogenesis. Cancer Cell *9*, 157–173.

Reyes-Mugica, M., Rieger-Christ, K., Ohgaki, H., Ekstrand, B.C., Helie, M., Kleinman, G., Yahanda, A., Fearon, E.R., Kleihues, P., and Reale, M.A. (1997). Loss of DCC expression and glioma progression. Cancer Res. *57*, 382–386.

Sonoda, I., Imoto, I., Inoue, J., Shibata, T., Shimada, Y., Chin, K., Imamura, M., Amagasa, T., Gray, J.W., Hirohashi, S., and Inazawa, J. (2004). Frequent silencing of low density lipoprotein receptor-related protein 1B (LRP1B) expression by genetic and epigenetic mechanisms in esophageal squamous cell carcinoma. Cancer Res. *64*, 3741–3747.

Suzuki, A., Yamaguchi, M.T., Ohteki, T., Sasaki, T., Kaisho, T., Kimura, Y., Yoshida, R., Wakeham, A., Higuchi, T., Fukumoto, M., et al. (2001). T cell-specific loss of Pten leads to defects in central and peripheral tolerance. Immunity *14*, 523–534.

Verhaak, R.G., Hoadley, K.A., Purdom, E., Wang, V., Qi, Y., Wilkerson, M.D., Miller, C.R., Ding, L., Golub, T., Mesirov, J.P., et al. (2010). Integrated genomic analysis identifies clinically relevant subtypes of glioblastoma characterized by abnormalities in PDGFRA, IDH1, EGFR, and NF1. Cancer Cell *17*, 98–110.

Wang, Y., Yang, J., Zheng, H., Tomasek, G.J., Zhang, P., McKeever, P.E., Lee, E.Y., and Zhu, Y. (2009). Expression of mutant p53 proteins implicates a lineage relationship between neural stem cells and malignant astrocytic glioma in a murine model. Cancer Cell *15*, 514–526.

Wei, Q., Clarke, L., Scheidenhelm, D.K., Qian, B., Tong, A., Sabha, N., Karim, Z., Bock, N.A., Reti, R., Swoboda, R., et al. (2006). High-grade glioma formation results from postnatal pten loss or mutant epidermal growth factor receptor expression in a transgenic mouse glioma model. Cancer Res. *66*, 7429–7437.

Wen, P.Y., and Kesari, S. (2008). Malignant gliomas in adults. N. Engl. J. Med. *359*, 492–507.

Xiao, A., Yin, C., Yang, C., Di Cristofano, A., Pandolfi, P.P., and Van Dyke, T. (2005). Somatic induction of Pten loss in a preclinical astrocytoma model reveals major roles in disease progression and avenues for target discovery and validation. Cancer Res. *65*, 5172–5180.

Yan, H., Parsons, D.W., Jin, G., McLendon, R., Rasheed, B.A., Yuan, W., Kos, I., Batinic-Haberle, I., Jones, S., Riggins, G.J., et al. (2009). IDH1 and IDH2 mutations in gliomas. N. Engl. J. Med. *360*, 765–773.

Yin, D., Ogawa, S., Kawamata, N., Tunici, P., Finocchiaro, G., Eoli, M., Ruckert, C., Huynh, T., Liu, G., Kato, M., et al. (2009). High-resolution genomic copy number profiling of glioblastoma multiforme by single nucleotide polymorphism DNA microarray. Mol. Cancer Res. *7*, 665–677.

Yue, Q., Groszer, M., Gil, J.S., Berk, A.J., Messing, A., Wu, H., and Liu, X. (2005). PTEN deletion in Bergmann glia leads to premature differentiation and affects laminar organization. Development *132*, 3281–3291.

Zarghooni, M., Bartels, U., Lee, E., Buczkowicz, P., Morrison, A., Huang, A., Bouffet, E., and Hawkins, C. (2010). Whole-genome profiling of pediatric diffuse intrinsic pontine gliomas highlights platelet-derived growth factor receptor alpha and poly (ADP-ribose) polymerase as potential therapeutic targets. J. Clin. Oncol. *28*, 1337–1344.

Zheng, H., Ying, H., Yan, H., Kimmelman, A.C., Hiller, D.J., Chen, A.J., Perry, S.R., Tonon, G., Chu, G.C., Ding, Z., et al. (2008). p53 and Pten control neural and glioma stem/progenitor cell renewal and differentiation. Nature *455*, 1129–1133.